Investigation of Micro-Columnar Scintillators on an Optical Fiber Coupled Compact Imaging System[1]

Martin P. Tornai[2], *Member, IEEE*, Caryl N. Brzymialkiewicz[2,3], Andrew G. Weisenberger[4], Randal Wojcik[4], Vladimir Popov[4], Stan Majewski[4], Cynthia E. Keppel[4,5], Craig S. Levin[6], *Member, IEEE*, Sameer V. Tipnis[7], Vivek V. Nagarkar[7]

[2]*Section of Nuclear Medicine, Department of Radiology, Duke University Medical Center, Durham, NC USA*
[3]*Department of Biomedical Engineering, Duke University, Durham, NC USA*
[4]*Detector Group, Thomas Jefferson National Accelerator Facility, Newport News, VA, USA*
[5]*Department of Nuclear & High Energy Physics, Hampton University, Hampton, VA, USA*
[6]*Departments of Radiology, University of California & VA Medical Centers, San Diego, CA, USA*
[7]*Radiation Monitoring Devices, Inc., Watertown, MA, USA*

Abstract

A compact imaging system with a novel front-end detector is under investigation and development. Unique aspects of this collimator-less system include the use of many thousands of micro-columnar (<10 μm diameter) CsI front-end scintillators (140 and 200 microns tall on faceplates of plane glass, fiber optics (FO), and FO with statistical extramural absorbers (EMA)) that are coupled through a 4 times reducing FO bundle to a metal-channel multianode position sensitive photo-detector. The highly discrete nature of the scintillator micro-column arrays ensures very fine intrinsic spatial resolution, limited by the particle penetration and backscatter in the detector assembly, while their retro-reflector-tipped front-ends facilitate light propagation towards the photo-detector. Monte Carlo simulations confirmed the limiting nature of particle penetration on measurable resolution. With this system, absolute light output was highest for the taller arrays, which contradicts results of using much larger, quantized scintillators in other applications. While MTF mea-surements with an x-ray source indicate the best response with the arrays on FO+EMA substrates, measurements with high and medium (1.7 MeV and 635 keV) energy beta line sources yield the best responses with the plane glass substrate indi-cating that energy thresholding affects resolution in the classical way, even with these highly miniaturized arrays. Further experiments of complex positron emission distri-butions along with large gamma ray backgrounds yield images with minimal background contamination and no distortions.

I. INTRODUCTION

Nuclear medicine based surgical guidance with non-imaging detector probes is gaining in acceptance and popularity. One drawback of non-imaging guidance is the lack of ancillary information of the surveyed area, e.g. distinction between two neighboring radioactive regions, which can be more easily distinguished with an intraoperative *imaging* probe with very fine spatial resolution. More complete and accurate tumor resection has been shown to increase the life span and improve the quality of life of surgically treated patients. This has been an underlying motivation in the development of beta and gamma sensitive imaging as well as non-imaging detectors [1], with this class of intra-operative *imaging* detectors specifically designed to help delineate the post-excisional tumor boundaries which a surgeon could subsequently identify and remove.

To date, positron emitting radiotracers (e.g. ^{18}F-fluoro-deoxyuridine, ^{18}F-FDG, and other compounds under development) whose annihilation γ's can also be imaged with PET promise an available means of intraoperatively imaging radiolabelled lesions and their boundaries. Direct β^+ detection, however, with the accompanying 511 keV annihilation γ backgrounds in the patient's body has been shown to degrade image contrast. Thus, a key aspect of this work, in contrast to earlier imaging work with lower-Z scintillators [2-4] or semiconductors [1,5], is that a considerably thinner and higher effective-Z and density scintillator is investigated here, since it's light output is considerably better than other available lower-Z scintillators, and since the elements themselves could be uniformly discretized to repeatable submillimeter sizes [6-9]. With these <10 μm discrete scintillator sizes, there is a high degree of light channeling in the scintillator, in contrast to the light spreading, hence resolution degradation, even seen with thin, continuous scintillator disks [3,4].

II. EXPERIMENTAL METHODS

A. Micro-Columnar Scintillators

We investigate thousands of custom vapor-deposited, micro-columnar CsI(Tl) scintillators (Z_{eff}= 54, ρ= 4.5 g/cm^3, λ_{max}= 540 nm, I= 54k ph/MeV, τ= 900 nsec, n= 1.78) arranged in a disk as the front-end beta/positron sensitive detector (Fig. 1). The actual CsI(Tl) micro-columns shown are

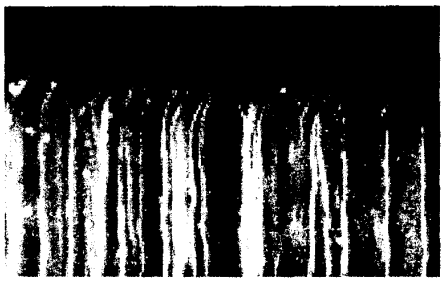

FIGURE 1. Scanning electron micrograph of the tops of a micro-columnar CsI(Tl) array similar to those used in the imaging system. Note the regularity of the ~6 μm diameter of each crystal as well as the retro-reflector like tips.

[1]This work was funded by NSF/MRI grant BES-9871378, grant RG-99-0305 from the Whitaker Foundation, and NIH grant RO1- CA76006.

0-7803-6503-8/01/$10.00 2001 IEE

TABLE 1
Physical characteristics of the <10 μm micro-columnar arrays.

Crytal Thickness (mm)	Array Dimensions (X x Y mm^2)	Substrate Material	Substrate Thickness (mm)
0.14	25.4 ϕ	FO + EMA	2.0
0.14	25.4 x 25.4	FO	1.0
0.14	25.4 x 25.4	Plano Glass	1.0
0.20	25.4 x 25.4	FO + EMA	2.0
0.20	25.4 x 25.4	FO	2.0
0.20	25.4 x 25.4	Plano Glass	1.0

~30 μm in height, and each CsI(Tl) element is ~6 μm in diameter. The parameters of the actually investigated large scintillator arrays containing ≤10 μm diameter micro-columnar scintillators are shown in Table 1.

The micro-columns are hermetically sealed with approximately 3-4 μm of sealant and an ~0.2 μm layer of reflective aluminum on the source entrance front-end, and are backed by a 1-2 mm thick borosilicate fiber-optic or glass backplate. The elements in the fiber-optic (FO) backplate consist of 10 μm diameter FO with a numerical aperture (NA) of 0.66, and include a statistical Extra Mural Absorber (EMA) that is used to absorb stray or scattered light that could spread through the FO backplate.

The conical peaks at the particle entrance ends (Fig. 1) act like retro-reflectors [10,11] and actually help to reflect scintillation light back down towards the photodetector, thus improving the light output of these long and thin scintillators. Note that each column of CsI(Tl) is truly a distinct element with small air gaps that enhance total internal reflection along their sides towards the photodetector.

B. Monte Carlo Simulations

Computer simulations, similar to those made for other scintillators [3,12], were performed to determine 3-dimensional distributions of ^{32}P (E_{max}= 1.71 MeV) beta and ^{18}F (E_{max}= 635 keV) positron particle tracks in 5 mm thick CsI scintillators. The simulated thickness was over-estimated from Continuous Slowing Down Approximation (CSDA) calculations to completely absorb the particles at these energies. The results of these simulations were compared with CSDA range and projected range calculations.

C. Fiber-Optic Tapered Coupling

The fiber optic reducing bundle (*Schott Fiber Optic, Inc.*, Southbridge, MA) nearly matches the scintillator at the front-end to the active surface of the position-sensitive (PS) PMT (Fig. 2). The fiber optic bundle reduces the 9 cm^2 front surface in area by a factor of 4 and consists of 10 μm fibers, with 1.0 NA. The reducing fiber-optic also includes an EMA similar to that used in the scintillator assembly. An additional 3 mm light diffuser was also included between the fiber optic bundle and the PSPMT to ensure that enough parallel channels received a signal from which to calculate the position of beta interaction.

D. PSPMT Electronics and Control

The PSPMT (model R5900-M64, *Hamamatsu Corp.*, Tokyo, Japan) has 64 parallel channels whose signals are divided by a custom built resistive divider to reduce the number of output signals from 64 to 16 (8 each in X and Y, respectively). The resistive divider acts to determine the center-of-gravity for the interactions in X and Y dimensions.

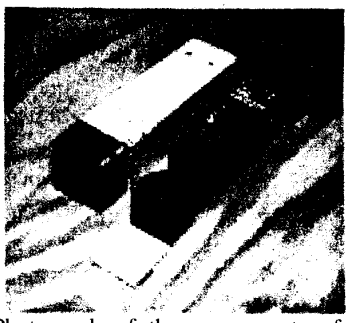

FIGURE 2. Photograph of the components of the compact imaging system. This shown scintillator array (lower right) consists of an 8x8 array of elements in white epoxy.

A discriminator signal is obtained by summing the 16 output signals above a noise threshold, and then generating a delayed and amplified 1.5 μsec gate with a custom NIM board to trigger the charge sensitive FERA ADCs (*Lecroy Research Systems, Inc.*, Chestnut Ridge, NY). All modules are under control by a G3 PowerMac laptop computer running Kmax data acquisition software (*Sparrow Corp.*, Starkville, MI) through SCSI.Readout of the list mode collected data is similar to that in [13].

E. Line Source & Phantom Measurements

Intrinsic line spread functions (LSF) were obtained for each scintillator array on a FO substrate by illuminating the arrays through a 10 μm tungsten slit with x-rays generated from a W target (model GX1000, *Gendex Corp.*). Acquisition parameters include: 40 kVp source energy, 1.25 sec exposure, source distance of 45 cm, CCD measurement system (*Photometrix*) using a 3:1 FO taper and had 14 bit dyanmic range. These LSFs were measured in the standard way for CCD calibration, and the MTFs were obtained as the Fourier transforms of the LSFs. Extrinsic LSF measurements of emission line sources made of thread («1 mm diam.) soaked in ~25 μCi solutions of ^{32}P and ^{18}F and suspended in air with a custom built C-clamp were acquired with the lines positioned horizontally and diagonally on the various crystal surfaces.

A custom built 1 cm thick acrylic transmission phantom (*Data Spectrum Corp.*, Hillsborough, NC) containing 6 sectors of holes (1.2, 1.5, 2.2, 3.0, 3.5, 4.0 mm diameters for each sector) spaced on twice their diameters was imaged with ^{32}P betas with all scintillator combinations. Some holes in the 1.5 and 2.2 mm sectors of the transmission phantoms were partially filled with 6 μCi and 4.9 μCi of ^{18}F activity in water, respectively, and sealed with one layer of clear tape. Emission images of these partially filled holes were obtained by themselves and also with 0.4 mCi of ^{18}F activity in 1.5 liters of water directly behind the positron emission source as a source of annihilation contamination.

III. RESULTS

A. Monte Carlo Particle Tracking

Monte Carlo simulations clearly demonstrate that the incident particles' penetration or range will play a more domi-

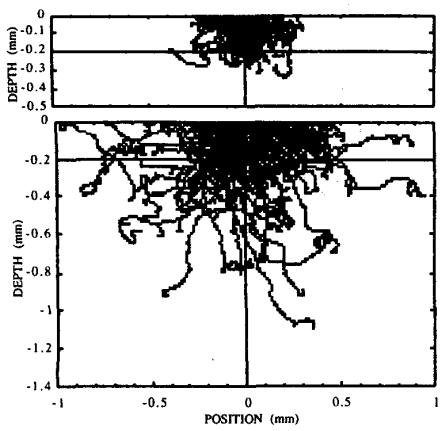

FIGURE 3. Monte Carlo particle tracking simulation results for (top) ^{18}F and (bottom) ^{32}P in thick CsI media. In both cases, the horizontal line delineates the maximum thickness of CsI used here, and the vertical line approximately represents the width of a single micro-columnar scintillator. Source origin is at (0,0).

nant role in spatial resolution degradation than the intrinsic 10 μm micro-scintillator size (Fig. 3). CSDA range calculations yield a maximum range (complete pathlength) of 920 μm for ^{18}F positrons and a projected range (maximum distance attained from source) of 460 μm, while the simulation results indicate values smaller than those calculated. Based on these particle tracking results, it might seem desirable to have scintillator thicknesses of ~400 μm to have a good efficiency for ^{18}F positrons. However, thicker beta detectors will be accompanied by larger annihilation backgrounds. Based on results of simulations and measurements of larger quantized CsI(Tl) scintillators [14,15] and the consequent decreased light output expected with longer, narrower discrete elements, we decided to initially test thinner scintillator arrays (Table 1).

B. Intrinsic & Extrinsic Spatial Resolution

The intrinsic MTFs of the measured arrays indicate that the shorter arrays with FO+EMA have a better frequency response than the other arrays (Fig. 4). This is not surprising given that there is less chance for light to spread, hence decrease the spatial resolution, within normally irradiated shorter crystals on a substrate that partially absorbs stray light. All MTFs were quite similar which also indicates that the highly discrete nature of the micro-columns plays a dominant role in determining the spatial response of the system. Note that the plano-glass substrate arrays had large tails that precluded adequate determination of the Fourier transforms of the LSFs.

Extrinsic measurements with ^{32}P on the assembled imaging system yielded large full widths at half maxima (FWHM) for the exposed emission line source (Figs. 5 and 6) most likely due to the large particle penetration in the detector (Fig. 3), and also due to backscatter of energetic particles a large distance away from the source [4]. There was an inverse trend in extrinsic spatial response to that of the intrinsic MTF measurements. That is, the arrays on substrates where higher light collection along with greater light spreading was expected (plano > FO > FO+EMA) yielded smaller measured FWHMs. This is consistent with the notion that spatial resolution is proportional to light intensity since the intrinsic measurements utilized an integrating current detector without

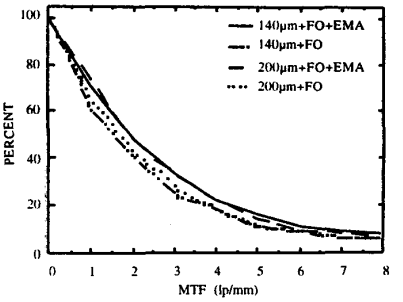

FIGURE 4. MTF results for some scintillator arrays on two substrates. The Nyquist frequency is 8.7 lp/mm.

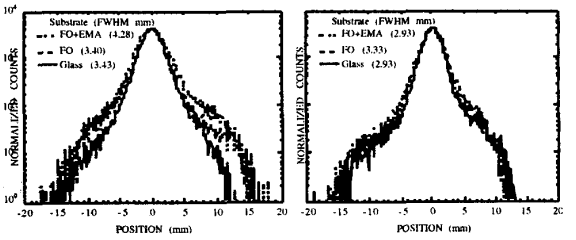

FIGURE 5. Semi-log plots of uncorrected emission LSFs for all arrays measured with a horizontal ^{32}P line source in air, directly on top of the (Left) 140 μm arrays and (Right) 200 μm arrays.

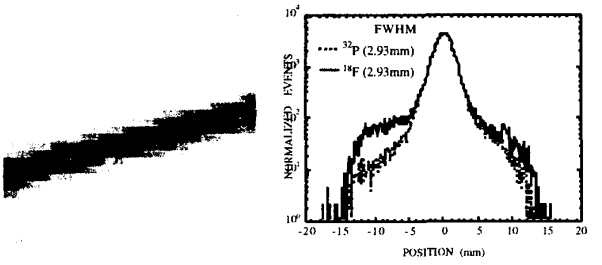

FIGURE 6. LSF image and profiles of the 200 μm array on the glass substrate. (Left) 32x32 corrected image (see *III.C.*) of the exposed ^{18}F line source. (Right) Superimposed, uncorrected LSFs of ^{18}F and ^{32}P. Note high tails in the ^{18}F spectrum, due to the presence of the annihilation background in the detector.

TABLE 2
Intrinsic measurement results of the scintillator arrays.

Crytal Thickness (mm)	Substrate Material	Relative Light Output	SNR
0.14	FO + EMA	0.34	143
0.14	FO	0.70	226
0.14	Plano Glass	0.70	245
0.20	FO + EMA	0.44	196
0.20	FO	1.00	325
0.20	Plano Glass	0.91	347

energy discirmination and the extrinsic measurements used a classical nuclear emission detector arrangement (see *II.D.*).

Measurements of relative light output and signal-to-noise ratios (SNRs) confirmed the relative signal intensities of the different arrays on various substrates (Table 2). Furthermore, the taller micro-columns were measured to have greater light output than the shorter ones, which contradicts measurements of larger (>1x1 mm^2), quantized scintillators [14,15].

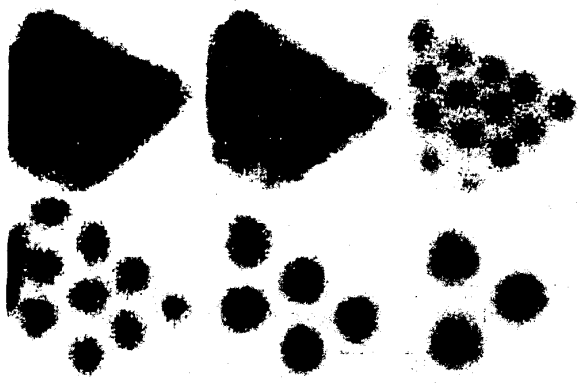

FIGURE 7. (From Left to Right, Upper to Lower) Uncorrected, raw images of ^{32}P transmission events through 1.2, 1.5, 2.2, 3.0, 3.5 and 4.0 mm holes spaced on twice their diameters.

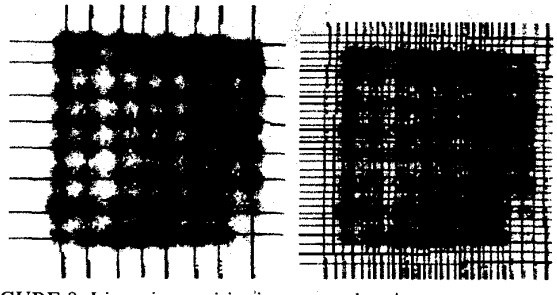

FIGURE 8. Linearity positioning maps showing raw, uncorrected images of 8x8 array of 1.5 mm diam. transmission holes. Superimposed on raw images are (Left) results of 2D peak-finding algorithm, and (Right) results of 2D valley finding algorithm, further subdivided to yield 32x32 pixellation.

C. *Transmission Imaging of Complex Phantoms*

Complex transmission distributions were imaged to empirically determine the ability to visualize juxtaposed regions of radioactivity (Fig. 7). While the extrinsic LSFs yielded <3 mm FWHMs, the smallest discernible hole spacing was 1.5 mm, indicating that the intrinsic system resolution was better than that value for the uncorrected data. These image results corroborate the earlier explanation for the large widths of the measured emission line sources.

Using the results of this image data (Fig. 7), an 8x8 transmission mask with 1.5 mm holes spaced on twice their diameters was constructed. This mask was then used to calibrate the linearity of the arrays in the imaging system (Fig. 8), and to use the discretization to obtain and incorporate uniformity and energy correction data. These are standard software-based NEMA-type calibrations that correct the list mode acquired data. While a drawback of this approach was that we were limited to a 32x32 pixellated subdivision of the raw (260x260 pixel) data, thus losing spatial resolution, each element in the corrected 32x32 image arrays contained independent position and spectral information about that immediate region. Thus, this holospectral information in the image data could be further exploited and optimized.

D. *Emission Imaging of Positron Distributions*

Images of complex positron emission distributions illustrate the resolution losses associated with 2π emissions directly on the detector surface (Fig. 9), as well as the resolution degradation due to presence of annihilation gamma backgrounds (Fig. 10). There was difficulty in discerning the 1.5 mm diameter wells, but visualization of the 2.3 mm wells with emission imaging indicates that the emission resolution is still better than that measured with the LSFs.

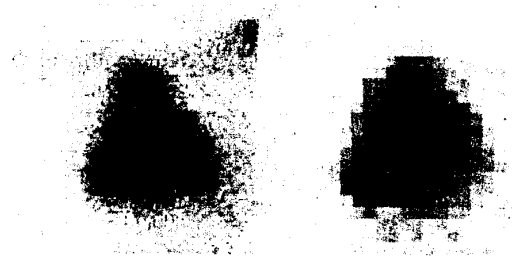

FIGURE 9. Cropped images of ~6 partially filled 1.5mm holes on 3.0 mm centers in (left) the raw, uncorrected image, and (right) the corrected image with 32x32 pixellation. Images acquired with 6.0 μCi ^{18}F activity plus 0.4 mCi gamma ray background.

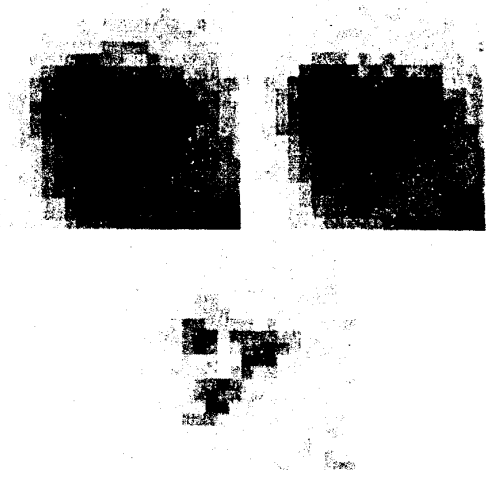

FIGURE 10. Cropped images of 3 partially filled 2.3 mm holes on 4.6 mm centers, with 4.9 μCi of ^{18}F activity. (Top, Left) Emission holes with 0.4 mCi gamma ray background; (Top, Right) emission holes without any additional background; (Bottom) Difference image illustrating spatial distribution of annihilation gamma ray signal only.

The addition of the gamma ray background immediately behind the positron emission source simulated expected clinical imaging conditions. While there is an apparent loss in spatial resolution, the signal degradation is more probably due to decreased image contrast. The difference image (Fig. 10) illustrates that the gamma ray contribution is fairly uniform over the detector surface, but also that there are focal spots that correspond to the locations of the emission sources. This is not surprising, since positrons detection liberates annihilation gammas in efficient positron detectors.

Furthermore, the distinction in energy spectra was minimal (Fig. 11, left) as the 511 keV gamma ray efficiency is low with these CsI(Tl) thicknesses. The thin detectors also facilitate incomplete energy deposition due to inefficiency for Compton scattered photons as well as Compton- and photoelectrons that are not completely stopped in the scintillator.

However, the energy response of the scintillator arrays did

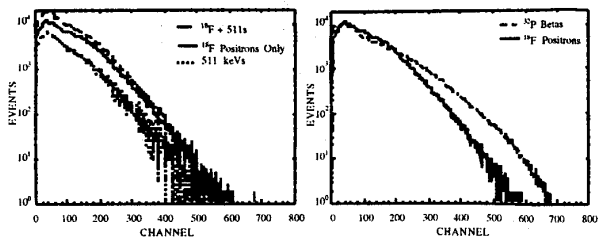

FIGURE 11. Semi-log plots of (Left) energy spectra from the data in Fig. 10 illustrating beta+gamma spectra, 'beta only' spectra, and the difference spectra representing the gamma only signal. (Right) Energy spectra illustrating differences between ^{32}P higher energy beta emissions and lower energy ^{18}F positron spectra.

distinguish between the lower and higher energy betas (Fig. 11, right). While the light output was not proportional to the factor of 2.7 difference between incident particle endpoint energies, the primary reason for this is due to the incomplete energy deposition from the higher energy, near minimum ionizing particles. This effect does not result in degraded system sensitivity, since partial energy deposition from any single event greater than threshold is still a valid event, but it affects the overall pulse height. Note also that for these thin scintillators and disparate incident particle energies, the higher endpoint energy particles will more uniformly deposit their energy along the length of the micro-columns, while the lower endpoint energy particles will predominantly deposit their energy near the incident surface. This factor can also influence the total light output from these long and very thin scintillators.

IV. Conclusions

A novel, compact imaging system was described that employs thousands of <10 μm diameter micro-columnar CsI(Tl) scintillators with FO coupling to the position sensitive PMT. The intrinsic (MTF) and extrinsic spatial responses were determined and found to be dependent on energy threshold, and also ultimately limited by the beta particle penetration rather than the intrinsic detector size. Monte Carlo particle tracking simulations confirmed the limiting effects on spatial resolution. With the best 200 μm scintillator array on the plano-glass substrate, the LSFs of particles of disparate energies, including additional annihilation backgrounds, were equivalent. Images of complex transmission phantoms indicate that the system resolution is <1.5 mm. This indicates that the 200 μm thin, high effective Z, high density scintillator would be an effective and efficient beta detector for various incident particles. Furthermore, emission images of complex distributions were clearly discernible and very sensitive to small quantities of ^{18}F activity. While the accompanying annihilation background slightly degraded image contrast, the overall 511 keV backgrounds had a small contribution to the energy spectrum, and pulse height differences were clearly discriminated between particles of various endpoint energies. One very interesting result of these measurements of ultra-thin and long micro-columnar scintillators was that for the sizes measured, the taller scintillators had higher light output and yielded better SNRs than the smaller scintillators, which seems to contradict measurements with larger scintillators with similar cross-sectional area to length ratios.

V. Acknowledgements

The authors thank the Duke University Medical Center Radiopharmacy and PET Cyclotron for providing the isotopes used in this study, and the Dept. of Radiology in the Durham Veterans Administration Hospital for providing facilities where the experiments were performed.

VI. References

[1] EJ Hoffman, MP Tornai, M Janecek, BE Patt, JS Iwanczyk. 1999. Intraoperative probes and imaging probes. [Review] *Eur. J. Nucl. Med.* **26**(8):913-935.

[2] LR MacDonald, MP Tornai, CS Levin, J Park, M Atac, DB Cline, EJ Hoffman. 1995. Investigation of the physical aspects of beta imaging probes using scintillating fibers and visible light photon counters. *IEEE Trans Nucl Sci.* **NS42**(4):1351-1360.

[3] CS Levin, LR MacDonald, MP Tornai, EJ Hoffman, J Park. 1996. Optimizing light collection from thin scintillators used in a beta-ray camera for surgical use. *IEEE Trans Nucl Sci.* **NS43**(3):2053-2060.

[4] MP Tornai, LR MacDonald, CS Levin, S Siegel, EJ Hoffman. 1996. Design considerations and initial performance of a 1.2 cm^2 beta imaging intra-operative probe. *IEEE Trans Nucl Sci.* **NS43**(4):2326-2335.

[5] MP Tornai, BE Patt, JS Iwanczyk, CR Tull, LR MacDonald, EJ Hoffman. A novel silicon array for intraoperative charged-particle imaging. Presented at *1998 IEEE NSS/MIC*, Toronto, Canada, 8-14 Nov. 1998.

[6] M Ito, M Yamaguchi, K Oba,. 1987. CsI(Na) scintillation plate with high spatial resolution. *IEEE Trans Nucl Sci.* **NS34**(1):401-405.

[7] VV Nagarkar, TK Gupta, SR Miller, Y Klugerman, MR Squillante, G Entine. 1998. Structured CsI(Tl) scintillators for x-ray imaging applications. *IEEE Trans Nucl Sci.* NS45(3):492-496.

[8] VV Nagarkar, SV Tipnis, TK Gupta, SR Miller, VB Gaysinskiy, Y Klugerman, MR Squillante, G Entine, WW Moses. 1999. High speed x-ray imaging camera using a tructured CsI(Tl) scintillator. *IEEE Trans Nucl Sci.* NS46(3):232-236.

[9] SV Tipnis, VV Nagarkar, VB Gaysinskiy, P O'Dougherty, Y Klugerman, SR Miller, G Entine. 1999. Large area CCD based imaging system for mammography. *1999 IEEE NSS & MIC Conference Record.*

[10]JS Karp, G Muehllehner. 1985. Performance of a position-sensitive scintillation detector. *Phys Med Biol.* **30**(7):643-655.

[11]J Strobel, NH Clinthorne, WLRogers, 1997. Design studies for a cesium iodide silicon photodiode gamma camera. *J Nucl Med.* **38**(5):31P-32P.

[12]CS Levin, EJ Hoffman. 1999. Calculation of positron range and its effect on the fundamental limit of positron emission tomography system spatial resolution. *Phys Med Biol.* **44**(3):781-99.

[13]S Avery, C Keppel, S Majewski, AG Weisenberger, R Wojcik, C Zorn. 1997. Small gamma imaging probe with millimeter spatial resolution. *1997 IEEE NSS & MIC Conference Record.*

[14]AJ Bird, T Carter, AJ Dean, D Ramsden, BM Swinyard. 1993. The optimisation of small CsI(Tl) gamma-ray detectors. *IEEE Trans Nucl Sci.* **NS40**(4):395-399.

[15]MP Tornai, CS Levin, LR MacDonald, EJ Hoffman. 1997. Investigation of crystal geometries for fiber coupled gamma imaging intra-operative probes. *IEEE Trans Nucl Sci* **NS44**(3):1254-1261.